

Data-driven peakon and periodic peakon travelling wave solutions of some nonlinear dispersive equations via deep learning

Li Wang and Zhenya Yan*

*Key Laboratory of Mathematics Mechanization, Academy of Mathematics and Systems Science,
Chinese Academy of Sciences, Beijing 100190, China*

School of Mathematical Sciences, University of Chinese Academy of Sciences, Beijing 100049, China

Abstract

In the field of mathematical physics, there exist many physically interesting nonlinear dispersive equations with peakon solutions, which are solitary waves with discontinuous first-order derivative at the wave peak. In this paper, we apply the multi-layer physics-informed neural networks (PINNs) deep learning to successfully study the data-driven peakon and periodic peakon solutions of some well-known nonlinear dispersion equations with initial-boundary value conditions such as the Camassa-Holm (CH) equation, Degasperis-Procesi equation, modified CH equation with cubic nonlinearity, Novikov equation with cubic nonlinearity, mCH-Novikov equation, b -family equation with quartic nonlinearity, generalized modified CH equation with quintic nonlinearity, and etc. These results will be useful to further study the peakon solutions and corresponding experimental design of nonlinear dispersive equations.

Key words: Nonlinear dispersive equation; initial-boundary value conditions; physics-informed neural networks; deep learning; data-driven

1 Introduction

The well-known nonlinear dispersive Camassa-Holm (CH) equation can be used to describe the propagation of shallow water waves, and deduced by using the distinct approaches such as the symmetry method [1], an asymptotic expansion directly in the Hamiltonian for Euler's equations [2], and the tri-Hamiltonian duality related to the Korteweg-de Vries equation [3]. The CH equation admitted the peaked travelling wave solutions (alias *peakons*, i.e., solitary waves with discontinuous first-order derivative at the wave peak) [2]. After that, much attention has been paid to some physically interesting nonlinear wave equations describing breaking waves and possessing the peakon solution in the form $u_t - u_{xxt} + F(u, u_x, u_{xx}, u_{xxx}) = 0$ such as the Degasperis-Procesi (DP) equation [4], b -family equation [5, 6], Fokas-Olver-Rosenau-Qiao (FORQ) equation (alias modified CH (mCH) equation) [3, 7, 8], mCH-CH equation [9], Novikov equation [10], mCH-Novikov equation [11], and etc. Up to now, it is still an interesting subject to study these nonlinear peakon equations via distinct approaches.

Recently, mechanics learning with deep neural networks plays a more and more important role in many fields [12, 13]. Particularly, various deep neural network learning approaches [14–22] have been paid more and more attention in the study of linear and nonlinear partial differential equations (PDEs). The physics-informed neural network (PINN) approach [21, 22] were presented, and has been applied to many linear and nonlinear PDEs [23–27], as well as other types of equations such as the fractional PDEs [28], and stochastic differential equations [29]. More recently, Shin, *et al* [30] theoretically showed the consistency of PINNs for the linear second-order elliptic and parabolic type PDEs.

In this paper, we would like to use the PINN deep learning to consider the Cauchy problem of the nonlinear dispersive equations with peakon solutions

$$\begin{cases} (1 - \partial_x^2)u_t + \mathcal{N}(u, u_x, u_{xx}, u_{xxx}, \dots) = 0, & x \in (L_1, L_2), \quad t \in (0, T), \\ u(x, 0) = u_0(x), & x \in [L_1, L_2], \\ u(L_1, t) = u(L_2, t), & t \in [0, T], \end{cases} \quad (1)$$

*Email address: zyyan@mmsrc.iss.ac.cn (Corresponding author)

where the subscripts denote the partial derivatives (e.g., $u_t = \partial u / \partial t$), $\partial_x = \partial / \partial x$, $\mathcal{N}(u, u_x, u_{xx}, u_{xxx}, \dots)$ is some nonlinear function of related variables such that Eq. (1) contains many famous nonlinear peakon equations, for example:

- i) The generalized b -family (gbf) equation with nonlinearities of degree $(k+1)$ [31–34]

$$(1 - \partial_x^2)u_t + u^k \omega_x + bu^{k-1}u_x \omega = 0, \quad \omega := u - u_{xx}, \quad k \in \mathbb{N}^+, \quad b \in \mathbb{R}, \quad (2)$$

which contains the well-known models: ia) the integrable CH equation [1, 2] for $k=1, b=2$

$$(1 - \partial_x^2)u_t + 3uu_x - 2u_x u_{xx} - uu_{xxx} = 0 \quad (3)$$

admitting the second-order Lax pair [2]; ib) the integrable DP equation [4] for $k=1, b=3$

$$(1 - \partial_x^2)u_t + 4uu_x - 3u_x u_{xx} - uu_{xxx} = 0, \quad (4)$$

which is related to a negative flow of the Kaup-Kupershmidt hierarchy by a reciprocal transformation, and admits the third-order Lax pair [5]; ic) the b -family equation [5, 6] for $k=1$

$$(1 - \partial_x^2)u_t + (b+1)uu_x - bu_x u_{xx} - uu_{xxx} = 0, \quad (5)$$

id) the Novikov equation with cubic nonlinearity [10] for $k=2, b=3$

$$(1 - \partial_x^2)u_t + 4u^2 u_x - 3uu_x u_{xx} - u^2 u_{xxx} = 0, \quad (6)$$

which is also completely integrable, and related to a negative flow in the Sawada-Kotera hierarchy by a reciprocal transformation, as well as admits the third-order Lax pair [35]; and ie) the modified Novikov equation [36] for $k=2$

$$(1 - \partial_x^2)u_t + (b+1)u^2 u_x - buu_x u_{xx} - u^2 u_{xxx} = 0; \quad (7)$$

- ii) The generalized modified Camassa-Holm (gmCH) equation with nonlinearities of degree $(2k+1)$ [37, 38]

$$(1 - \partial_x^2)u_t + [(u^2 - u_x^2)^k (u - u_{xx})]_x = 0, \quad k \in \mathbb{N}^+, \quad (8)$$

containing the integrable FORQ equation [3, 7, 8] (or the mCH equation) with cubic nonlinearity for $k=1$

$$(1 - \partial_x^2)u_t + [(u^2 - u_x^2)(u - u_{xx})]_x = 0, \quad (9)$$

which is also completely integrable, and admits the second-order Lax pair [8].

- iii) The generalized mCH and b -family equation with nonlinearities of degree $\max\{2k+1, s+1\}$

$$(1 - \partial_x^2)u_t + k_1[(u^2 - u_x^2)^k \omega]_x + k_2(u^s \omega_x + bu^{s-1}u_x \omega) = 0, \quad k, s \in \mathbb{N}^+, \quad (10)$$

containing iiiia) the mCH-CH equation for $k=s=1, b=2$ [9]

$$(1 - \partial_x^2)u_t + k_1[(u^2 - u_x^2)\omega]_x + k_2(u\omega_x + 2u_x \omega) = 0, \quad k_1, k_2 \in \mathbb{R}, \quad (11)$$

and iiib) the mCH-Novikov equation with cubic nonlinearity [11]

$$(1 - \partial_x^2)u_t + k_1[(u^2 - u_x^2)\omega]_x + k_2(u^2 \omega_x + 3uu_x \omega) = 0, \quad k_1, k_2 \in \mathbb{R}, \quad (12)$$

- iv) The combination of generalized mCH and b -family equations

$$(1 - \partial_x^2)u_t + \sum_{k=1}^N k_j [(u^2 - u_x^2)^k \omega]_x + \sum_{s=1}^M k_s (u^s \omega_x + bu^{s-1}u_x \omega) = 0, \quad (13)$$

v) The general family of nonlinear peakon equations [38]

$$(1 - \partial_x^2)u_t + f_1(u, u_x)\omega + (f_2(u, u_x)\omega)_x = 0, \quad (14)$$

where f_j 's are some functions of u and u_x .

Notice that i) The generalized b -family equation (2) containing the CH equation (3), DP equation (4), b -family equation (5), and Novikov equation (6), possesses the peakon solution $u(x, t) = c^{1/k}e^{-|x-ct|}$, and periodic peakon solution $u(x, t) = c^{1/k} \operatorname{sech} \pi p(x)$ with $p(x) = \cosh(x - ct - 2\pi[(x - ct)/(2\pi)] - \pi)$ and $[\cdot]$ denoting the floor function or the greatest integer function [31–34]; ii) The mCH equation (9) has the peakon solution [39] $u(x, t) = \sqrt{3c/2}e^{-|x-ct|}$, $c > 0$ and periodic peakon solution [40] $u(x, t) = \sqrt{3c/(2 \cosh^2 \pi + 1)}p(x)$, $c > 0$; iii) The mCH-Novikov equation (12) has the peakon solution [11] $u(x, t) = \sqrt{3c/(2k_1 + 3k_2)}e^{-|x-ct|}$ and periodic peakon solution $u(x, t) = \sqrt{3c/[k_1(2 \cosh^2 \pi + 1) + 3k_2 \cosh^2 \pi]}p(x)$; iv) The generalized mCH equation (8) with $k = 2$ has the peakon solution [41] $u(x, t) = \sqrt[4]{15c/8}e^{-|x-ct|}$ and periodic peakon solution $u(x, t) = \sqrt[4]{15c/[\sinh \pi(8 \cosh^4 \pi + 4 \cosh^2 \pi + 3)]}p(x)$.

In this paper, we would like to consider the data-driven peakon and periodic peak solutions of the above-mentioned some physical interesting nonlinear PDEs via deep learning. The rest of this paper is arranged as follows: In Sec. 2, we introduce the PINN deep learning approach for the Cauchy problem of nonlinear PDEs (1). In Sec. 3, we use the PINN deep learning scheme to investigate the data-driven peakon and periodic peakon solutions of some famous nonlinear PDEs such as the CH equation (3), DP equation (4), Novikov equation (6), b -family equation (2) with $b = k = 3$, mCH equation (9), generalized mCH equation (8) with $k = 2$, mCH-CH equation (11), and the mCH-Novikov equation (12). In Sec. 4, we give some conclusions and discussions.

2 The PINN deep learning scheme of Eq. (1)

For the given Cauchy problem (1) we consider the residual PINN $f(x, t)$ as

$$f(x, t) := (1 - \partial_x^2)\hat{u}_t + \mathcal{N}(\hat{u}, \hat{u}_x, \hat{u}_{xx}, \hat{u}_{xxx}, \dots), \quad (15)$$

where $\mathcal{N}(\hat{u}, \hat{u}_x, \hat{u}_{xx}, \hat{u}_{xxx}, \dots)$ can be chosen as the some physical models mentioned in Sec. 1, a deep neural network $\hat{u}(x, t; w, b)$ denotes the continuous latent function with two families of network parameters: the weights w and biases b , and can be used to approximate $u(x, t)$ such that one can consider its partial derivatives of arbitrary order with respect to its input with the aid of automatic differentiation (e.g., Tensorflow) [42, 43], which differs from the numerical or symbolic differentiation. And then the residual PINN $f(x, t)$ given by Eq. (15) can also be found.

Therefore, with the aid of L-BFGS optimization method [44], the common parameters in the latent function $\hat{u}(x, t)$ and residual PINN $f(x, t)$ can be trained by using the multi-hidden-layer deep NN with some neurons per layer combined with a hyperbolic tangent activation function and minimizing the whole mean squared error (MSE) loss in the form

$$MSE = MSE_{ie} + MSE_b + MSE_f, \quad (16)$$

where

$$MSE_{ie} = \frac{1}{N_{int}} \sum_{j=1}^{N_{int}} \left| \hat{u}(x_0^j, 0) - u(x_0^j, 0) \right|^2 + \frac{1}{N_{end}} \sum_{j=1}^{N_{end}} \left| \hat{u}(x_T^j, T) - u(x_T^j, T) \right|^2, \quad (17)$$

$$MSE_b = \frac{1}{N_b} \sum_{j=1}^{N_b} \left(\left| \hat{u}(L_1, t_b^j) - u(L_1, t_b^j) \right|^2 + \left| \hat{u}(L_2, t_b^j) - u(L_2, t_b^j) \right|^2 + \left| \hat{u}(L_1, t_b^j) - \hat{u}(L_2, t_b^j) \right|^2 \right), \quad (18)$$

$$MSE_f = \frac{1}{N_f} \sum_{j=1}^{N_f} \left| f(x_f^j, t_f^j) \right|^2, \quad (19)$$

the observed measurements $\{\widehat{u}(x_0^j, 0)\}_1^{N_{int}}$ and $\{\widehat{u}(x_T^j, T)\}_1^{N_{end}}$ of the hidden field $\widehat{u}(x, t)$ are linked with the sampled initial and end training data $\{x_0^j, u(x_0^j, 0)\}_1^{N_{int}}$ and $\{x_T^j, u(x_T^j, T)\}_1^{N_{end}}$, respectively. $\{\widehat{u}(L_{1,2}, t_b^j)\}_1^{N_b}$ connect the selected boundary training data $\{t_b^j, u(L_{1,2}, t_b^j)\}_1^{N_b}$, and $\{x_f^j, t_f^j\}_1^{N_f}$ are connected with the marked points for the PINN $f(x, t)$. As a result, for the randomly chosen points, MSE_{ie} , and MSE_b represent the MSE losses of initial-end and periodic boundary data, respectively, and MSE_f is associated with the MSE loss of the PINN (15). The aims of MSE_{ie} and MSE_b try to match the learning solution to exact one for the initial and end data, and boundary data, respectively. The aim of MSE_f is to make the hidden $\widehat{u}(x, t)$ satisfy the considered physical equation (1).

In what follows we would like to use the PINN deep learning scheme to investigate the data-driven peakon and periodic peakon solutions of some famous nonlinear PDEs such as the CH equation (3), DP equation (4), Novikov equation (6), b -family equation (2) with $b = k = 3$, mCH equation (9), generalized mCH equation (8) with $k = 2$, mCH-CH equation (11), and the mCHN equation (12).

3 The data-driven peakon and periodic peakon solutions

3.1 The CH equation

In the subsection, we use the above-mentioned PINN deep learning approach to consider the data-driven peakon and periodic peakon solutions of the initial-boundary value problem of the CH equation given by Eqs. (1) and (3).

Case 1. For the peakon solution [2] $u(x, t) = ce^{-|x-ct|}$ of the CH equation (3), it is easy to see that when $c > 0$, the peakon solution is a *right-going* travelling wave solution, and bright peakon solution, whereas $c < 0$, it is a *left-going* travelling wave solution, and dark peakon solution. We here consider the stationary peakon solution at $t = 0$ as the initial condition

$$u(x, 0) = ce^{-|x|}, \quad x \in [-L, L], \quad (20)$$

and the periodic boundary condition $u(-L, t) = u(L, t)$. The considered residual PINN $f_{ch}(x, t)$ is written as

$$f_{ch}(x, t) := u_t - u_{xxt} + 3uu_x - 2u_xu_{xx} - uu_{xxx}. \quad (21)$$

Here, the hidden neural network $\widehat{u}(x, t)$ in Python can be defined as

```
def u(x, t):
    u = neural_net(tf.concat([x, t], 1), weights, biases)
    return u
```

such that the residual PINN $f_{ch}(x, t)$ in Python is written as

```
def f_ch(x, t):
    u = u(x, t)
    u_t = tf.gradients(u, t)[0]
    u_x = tf.gradients(u, x)[0]
    u_xx = tf.gradients(u_x, x)[0]
    u_xxt = tf.gradients(u_xx, t)[0]
    u_xxx = tf.gradients(u_xx, x)[0]
    f_ch = u_t - u_xxt + 3*u*u_x - 2*u_x*u_xx - u*u_xxx
    return f_ch
```

i) For the case $c > 0$ in the initial condition (20), i.e., the bright peakon solution, we take $c = 0.8$ and use the Fourier pseudo-spectral method [45] (i.e., one can take Fourier transform in space, and choose the explicit fourth-order Runge-Kutta method in time) to simulate the CH equation (3) with the initial value condition (20) and periodic boundary condition. The spatial region is $x \in [-6, 6]$ with 512 Fourier modes, and the temporal region is $t \in [0, 2]$ with time-step $\Delta t = 0.004$. As a consequence, we produce the data-set for the PINN pertaining

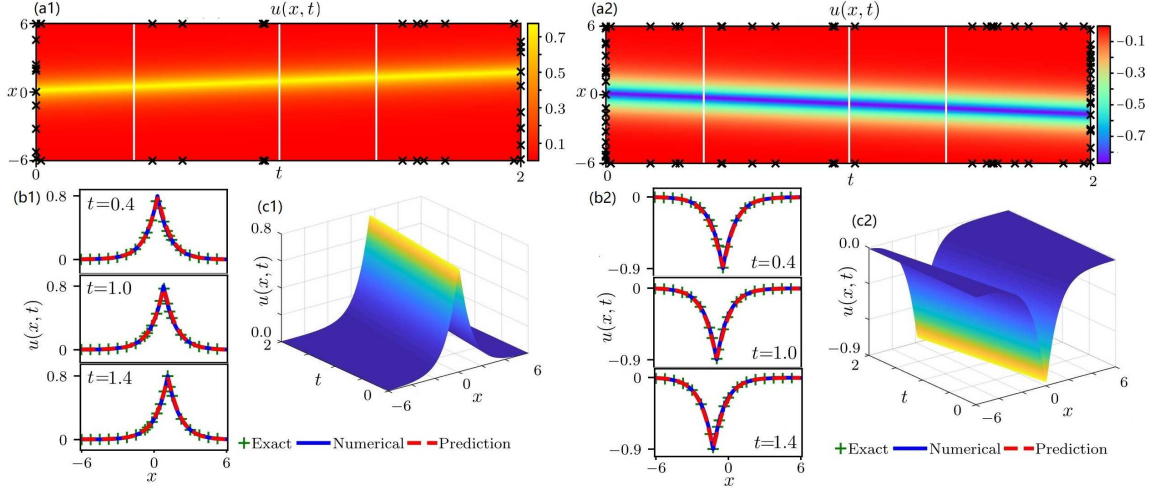


Figure 1: The CH equation. (a1,a2) The data-driven peakon solutions resulted from the PINN; (b1,b2) The comparisons between the learning, numerical, and exact peakon solutions at the distinct times $t = 0.4, 1, \text{ and } 1.4$; The \mathbb{L}_2 -norm errors $\hat{u}(x, t)$ between learning and numerical peakon solutions are (b1) $2.73\text{e-}02$ and (b2) $4.62\text{e-}02$; (c1,c2) The 3D profiles of the learning bright and dark peakon solutions. $c = 0.8$ for (a1, b1, c1) and $c = -0.9$ for (a2, b2, c2).

to the CH equation. The training data-set used in the PINN $f_{ch}(x, t)$ consists of randomly chosen $N_{int} = 10$ points from the initial data $u(x, 0)$, $N_{end} = 10$ points from the end data $u(x, 2)$, $N_b = 10$ points pertaining to the periodic boundary data, and $N_f = 1000$ points from the spatial-temporal solution zone.

Figures 1(a1) and (c1) exhibit the two-dimensional (2D) and three-dimensional (3D) profiles of the latent bright-peakon solution $\hat{u}(x, t)$ learned by a 5-hidden-layer deep PINN $f_{ch}(x, t)$ with 20 neurons per layer combined with a hyperbolic tangent activation function, and minimizing the MSE loss (16). The comparison of learning solution (red dashed line), numerical solution (blue solid line) and exact solution (green plus) is shown at three different times $t = 0.4, 1.0, \text{ and } 1.4$ (see Fig. 1(b1)). The \mathbb{L}_2 -norm error between learning solution $\hat{u}(x, t)$ and numerical solution is $2.73\text{e-}02$.

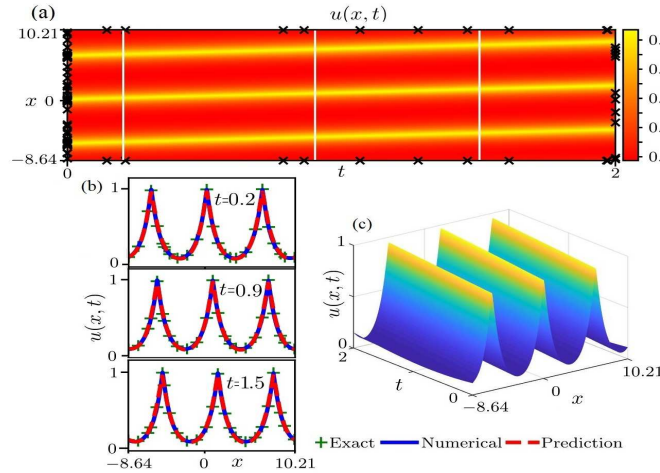


Figure 2: The CH equation: (a, c) The data-driven periodic peakon solution resulted from the PINN; (b) The comparisons between the learning, numerical, and exact periodic peakon solutions at the distinct times $t = 0.2, 0.9, \text{ and } 1.5$. The \mathbb{L}_2 -norm error between the learning and numerical periodic peakon solutions is $3.56\text{e-}02$.

ii) For the case $c < 0$ in the initial condition (20), i.e., dark peakon solution, we take $c = -0.9$ and use the same pseudo-spectral approach to produce the data-set for PINN pertaining to the CH equation in the spatio-temporal region $(x, t) \in [-6, 6] \times [0, 2]$ with the 512 Fourier modes in the x direction and time-step $\Delta t = 0.004$. The training data-set used in the PINN consists of randomly chosen $N_{int} = 20$ points from the initial data $u(x, 0)$, $N_{end} = 20$ points from the end data $u(x, 2)$, $N_b = 20$ points pertaining to the periodic boundary data, and $N_f = 1000$ points from the spatio-temporal solution zone. Figures 1(a2) and (c2) exhibit the 2D and 3D profiles of the latent dark-peakon solution $\hat{u}(x, t)$ learned by a 6-hidden-layer deep PINN with 20 neurons per layer combined with a hyperbolic tangent activation function. The comparison of learning solution (red dashed line), numerical solution (blue solid line) and exact solution (green plus) is shown at three different times $t = 0.4, 1.0, \text{ and } 1.4$ (see Fig. 1(b2)). The \mathbb{L}_2 -norm error between learning solution $\hat{u}(x, t)$ and numerical solution is $4.62\text{e-}02$.

Case 2. For the periodic peakon solution [32] $u(x, t) = c \operatorname{sech} \pi \cosh(x - ct - 2\pi \lfloor (x - ct)/(2\pi) \rfloor - \pi)$ of the CH equation (3), we consider the stationary periodic peakon solution at $t = 0$ as the initial value condition

$$u(x, 0) = c \operatorname{sech} \pi \cosh \left(x - 2\pi \left\lfloor \frac{x}{2\pi} \right\rfloor - \pi \right), \quad x \in [L_1, L_2] \quad (22)$$

and the periodic boundary $u(L_1, t) = u(L_2, t)$, as well as $c = 1$. Similarly, we use the pseudo-spectral approach to generate the data-set for the PINN pertaining to the CH equation in the spatio-temporal region $(x, t) \in [-8.64, 10.21] \times [0, 2]$ with the 512 Fourier modes in the x direction and time-step $\Delta t = 0.004$. The training data-set used in the PINN consists of randomly chosen $N_{int} = 60$ points from the initial data $u(x, 0)$, $N_{end} = 10$ points from the end data $u(x, 2)$, $N_b = 10$ points pertaining to the periodic boundary data, and $N_f = 1100$ points from the spatio-temporal solution zone. The hidden solution $\hat{u}(x, t)$ is learned by a 6-hidden-layer deep PINN $f_{ch}(x, t)$ with 40 neurons per layer combined with a hyperbolic tangent activation function.

Figures 2(a) and (c) exhibit the 2D and 3D profiles of the latent periodic peakon solution $\hat{u}(x, t)$. The comparison of learning solution (red dashed line), numerical solution (blue solid line) and exact solution (green plus) is shown at three different times $t = 0.2, 0.9, \text{ and } 1.5$ (see Fig. 2(b)). The \mathbb{L}_2 -norm error between learning solution $\hat{u}(x, t)$ and numerical solution is $3.56\text{e-}02$.

Similarly, the data-driven peakon and periodic peakon solutions of the DP equation (4) are also studied in **Appendix A**.

3.2 The Novikov equation with cubic nonlinearity

In the subsection, we use the PINN to consider the data-driven peakon solutions of the initial-boundary value problem of the Novikov equation with cubic nonlinearity (6).

Case 1. For the peakon solution [35] $u(x, t) = \sqrt{c} e^{-|x-ct|}$ with $c > 0$ of the Novikov equation (6), which is a *right-going* travelling wave solution, and bright peakon solution. It follows from the peakon solutions of CH and Novikov equations that for the right-going travelling wave with the same velocity, i) when $c > 1$, the amplitude of the CH peakon solution is larger than one of the Novikov peakon solution; when $0 < c < 1$, the amplitude of the CH peakon solution is smaller than one of the Novikov peakon solution; iii) when $c = 1$, the amplitudes of the CH and Novikov peakon solutions are same. We here consider the stationary peakon solution at $t = 0$ as the initial condition

$$u(x, 0) = \sqrt{c} e^{-|x|}, \quad x \in [-L, L] \quad (23)$$

and the periodic boundary $u(-L, t) = u(L, t)$. The considered PINN $f_{nov}(x, t)$ is written as

$$f_{nov}(x, t) := u_t - u_{xxt} + 4u^2 u_x - 3u u_x u_{xx} - u^2 u_{xxx}. \quad (24)$$

We here choose $c = 0.36$ in the initial condition (23), and use the Fourier pseudo-spectral method (i.e., one can take Fourier transform in space, and choose the explicit fourth-order Runge-Kutta method in time) to simulate the Novikov equation with the initial value condition (23) and periodic boundary condition. The spatial region is

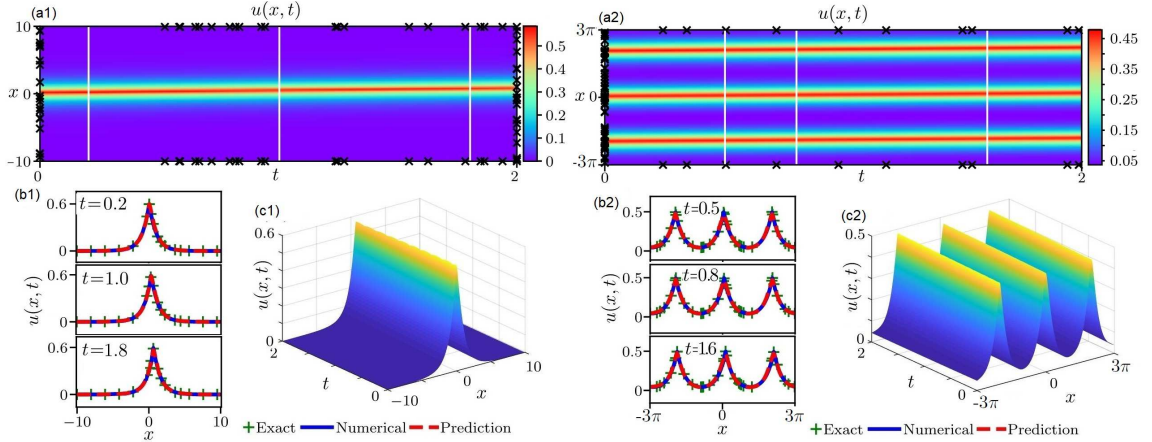


Figure 3: The Novikov equation. The data-driven peakon (a1,c1) and periodic peakon (a2, c2) solutions resulted from the PINN; (b1, b2) The comparisons between the learning, numerical, and exact peakon or periodic peakon solutions at the distinct times (b1) $t = 0.2, 1,$ and $1.8,$ or (b2) $t = 0.5, 0.8,$ and $1.6.$ The \mathbb{L}_2 -norm errors between the learning and numerical solutions are (b1) $3.82\text{e-}02$ and (b2) $4.56\text{e-}02.$ $c = 0.36$ for (a1,b1,c1), and $c = 0.25$ for (a2,b2,c2).

$x \in [-10, 10]$ with 256 Fourier modes, and the temporal region is $t \in [0, 2]$ with time-step $\Delta t = 0.004.$ As a result, we produce the data-set for the PINN pertaining to the Novikov equation. The training data-set used in the PINN $f_{nov}(x, t)$ consists of randomly chosen $N_{int} = 20$ points from the initial data $u(x, 0),$ $N_{end} = 20$ points from the end data $u(x, 2),$ $N_b = 20$ points pertaining to the periodic boundary data, and $N_f = 1000$ points from the spatio-temporal solution zone. Figures 3(a1) and (c1) exhibit the 2D and 3D profiles of the latent bright peakon solution $\hat{u}(x, t)$ learned by a 6-hidden-layer deep PINN $f_{nov}(x, t)$ with 20 neurons per layer combined with a hyperbolic tangent activation function. The comparison of learning solution (red dashed line), numerical solution (blue solid line) and exact solution (green plus) is shown at three different times $t = 0.2, 1.0$ and 1.8 (see Fig. 3(b1)). The \mathbb{L}_2 -norm error between learning solution $\hat{u}(x, t)$ and numerical solution is $3.82\text{e-}02.$

Case 2. For the periodic peakon solution [32, 46] $u(x, t) = \sqrt{c} \operatorname{sech} \pi \cosh(x - ct - 2\pi[(x - ct)/(2\pi)] - \pi)$ of the Novikov equation (6), we consider the stationary periodic peakon solution at $t = 0$ as the initial value condition

$$u(x, 0) = \sqrt{c} \operatorname{sech} \pi \cosh \left(x - 2\pi \left\lfloor \frac{x}{2\pi} \right\rfloor - \pi \right), \quad (25)$$

and the periodic boundary $u(-L, t) = u(L, t),$ as well as $c = 0.25.$ Similarly, we use the pseudo-spectral approach to generate the data-set for the PINN pertaining to the Novikov equation in the spatio-temporal region $(x, t) \in [-3\pi, 3\pi] \times [0, 2]$ with the 512 Fourier modes in the x direction and time-step $\Delta t = 0.004.$ The training data-set used in the PINN consists of randomly chosen $N_{int} = 70$ points from the initial data $u(x, 0),$ $N_{end} = 0$ point from the end data $u(x, 2),$ $N_b = 10$ points pertaining to the periodic boundary data, and $N_f = 2000$ points from the spatio-temporal solution zone. The hidden solution $\hat{u}(x, t)$ is learned by a 6-hidden-layer deep PINN $f_{nov}(x, t)$ with 20 neurons per layer combined with a hyperbolic tangent activation function.

Figures 3(a2) and (c2) exhibit the 2D and 3D profiles of the latent solution $\hat{u}(x, t)$ learned by a 6-hidden-layer deep PINN $f_{nov}(x, t)$ with 20 neurons per layer combined with a hyperbolic tangent activation function. The comparison of learning solution (red dashed line), numerical solution (blue solid line) and exact solution (green plus) is shown at three different times $t = 0.5, 0.8$ and 1.6 (see Fig. 3(b2)). The \mathbb{L}_2 -norm error between learning solution $\hat{u}(x, t)$ and numerical solution is $4.56\text{e-}02.$

3.3 The generalized b -family equation with quartic nonlinearity

In the subsection, we use the PINN to consider the data-driven peakon solutions of the initial-boundary value problem of the generalized b -family equation (2) with quartic nonlinearity for $b = k = 3.$

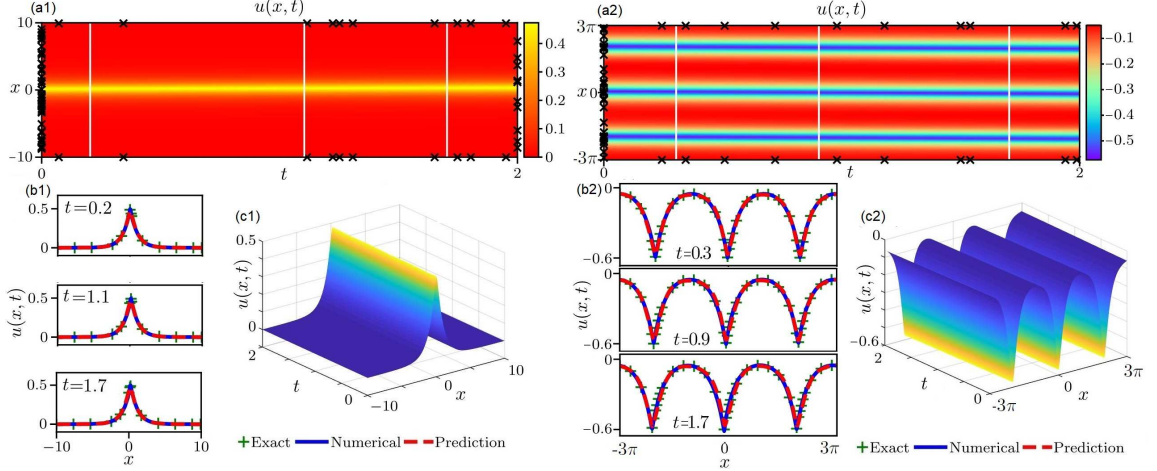


Figure 4: The generalized b -family equation (2) with $b = k = 3$. The data-driven peakon (a1,c1) and periodic peakon (a2, c2) solutions resulted from the PINN; (b1, b2) The comparisons between the learning, numerical, and exact peakon or periodic peakon solutions at the distinct times (b1) $t = 0.2, 1.1$, and 1.7 , or (b2) $t = 0.3, 0.9$, and 1.7 . The \mathbb{L}_2 -norm errors between the learning and numerical solutions are (b1) $4.62\text{e-}02$ and (b2) $6.2\text{e-}02$. $c = 0.125$ for (a1,b1,c1), and $c = -0.216$ for (a2,b2,c2).

Case 1. The generalized b -family equation (2) with $b = k = 3$ has the peakon solution [32] $u(x, t) = c^{1/3} e^{-|x-ct|}$. When $c > 0$, the peakon solution is a *right-going* travelling wave solution, and bright peakon solution, whereas $c < 0$, it is a *left-going* travelling wave solution, and dark peakon solution. We here consider the stationary peakon solution at $t = 0$ as the initial condition

$$u(x, 0) = c^{1/3} e^{-|x|}, \quad (26)$$

and the periodic boundary $u(-L, t) = u(L, t)$. The considered PINN $f_{gbf}(x, t)$ is written as

$$f_{gbf}(x, t) := u_t - u_{xxt} + 4u^3 u_x - 3u^2 u_x u_{xx} - u^3 u_{xxx}. \quad (27)$$

We here consider $c = 0.125$ in the initial condition (26), and use the Fourier pseudo-spectral method (i.e., one can take Fourier transform in space, and choose the explicit fourth-order Runge-Kutta method in time) to simulate the generalized b -family equation (2) with $b = k = 3$, the initial value condition (26), and periodic boundary condition. The spatial region is $x \in [-10, 10]$ with 256 Fourier modes, and the temporal region is $t \in [0, 2]$ with time-step $\Delta t = 0.004$. As a result, we produce the data-set for the PINN pertaining to the generalized b -family equation (2) with quartic nonlinearity for $b = k = 3$. The training data-set used in the PINN $f_{gbf}(x, t)$ consists of randomly chosen $N_{int} = 40$ points from the initial data $u(x, 0)$, $N_{end} = 10$ points from the end data $u(x, 2)$, $N_b = 10$ points pertaining to the periodic boundary data, and $N_f = 3000$ points from the spatio-temporal solution zone. Figures 4(a1) and (c1) exhibit the 2D and 3D profiles of the latent solution $\hat{u}(x, t)$ learned by a 5-hidden-layer deep PINN $f_{gbf}(x, t)$ with 20 neurons per layer combined with a hyperbolic tangent activation function. The comparison of learning solution (red dashed line), numerical solution (blue solid line) and exact solution (green plus) is shown at three different times $t = 0.2, 1.1$ and 1.7 (see Fig. 4(b1)). The \mathbb{L}_2 -norm error between learning solution $\hat{u}(x, t)$ and numerical solution is $4.62\text{e-}02$.

Case 2. The generalized b -family equation (2) with $b = k = 3$ has the periodic peakon solution [32] $u(x, t) = c^{1/3} \operatorname{sech} \pi \cosh(x - ct - 2\pi[(x - ct)/(2\pi)] - \pi)$, we consider the stationary periodic peakon solution at $t = 0$ as the initial value condition

$$u(x, 0) = c^{1/3} \operatorname{sech} \pi \cosh \left(x - 2\pi \left\lfloor \frac{x}{2\pi} \right\rfloor - \pi \right), \quad (28)$$

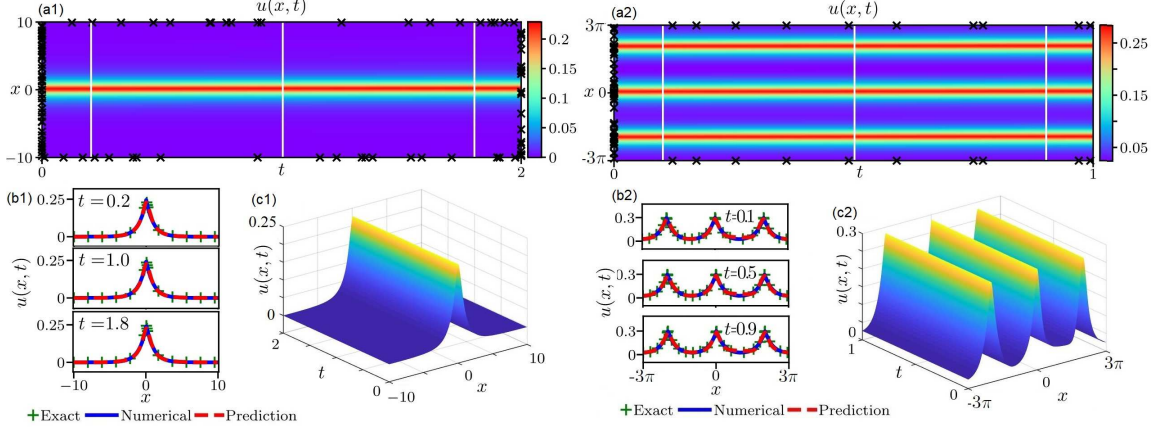


Figure 5: The mCH equation (9). The data-driven peakon (a1,c1) and periodic peakon (a2, c2) solutions resulted from the PINN; (b1, b2) The comparisons between the learning, numerical, and exact peakon or periodic peakon solutions at the distinct times (b1) $t = 0.2, 1, \text{ and } 1.8$, or (b2) $t = 0.1, 0.5, \text{ and } 0.9$. The \mathbb{L}_2 -norm errors between the learning and numerical solutions are (b1) $4.74\text{e-}02$ and (b2) $4.09\text{e-}02$. $c = 0.04$ for (a1,b1,c1), and $c = 0.06$ for (a2,b2,c2).

and the periodic boundary $u(L_1, t) = u(L_2, t)$, as well as $c = -0.216$. Similarly, we use the pseudo-spectral approach to generate the data-set for the PINN pertaining to the generalized b -family equation (2) with $b = k = 3$ in the spatio-temporal region $(x, t) \in [-3\pi, 3\pi] \times [0, 2]$ with the 512 Fourier modes in the x direction and time-step $\Delta t = 0.004$. The training data-set used in the PINN consists of randomly chosen $N_{int} = 50$ points from the initial data $u(x, 0)$, $N_{end} = 0$ point from the end data $u(x, 2)$, $N_b = 10$ points pertaining to the periodic boundary data, and $N_f = 2000$ points from the spatio-temporal solution zone. The hidden solution $\hat{u}(x, t)$ is learned by a 6-hidden-layer deep PINN $f_{gbf}(x, t)$ with 20 neurons per layer combined with a hyperbolic tangent activation function.

Figures 4(a2) and (c2) exhibit the 2D and 3D profiles of the latent solution $\hat{u}(x, t)$ learned by a 6-hidden-layer deep PINN $f_{gbf}(x, t)$ with 20 neurons per layer combined with a hyperbolic tangent activation function. The comparison of learning solution (red dashed line), numerical solution (blue solid line) and exact solution (green plus) is shown at three different times $t = 0.3, 0.9$ and 1.7 (see Fig. 4(b2)). The \mathbb{L}_2 -norm error between learning solution $\hat{u}(x, t)$ and numerical solution is $6.2\text{e-}02$.

3.4 The mCH equation with cubic nonlinearity

In the subsection, we use the PINN to consider the data-driven peakon solutions of the initial-boundary value problem of the mCH equation (9).

Case 1. For the peakon solution [39] $u(x, t) = \sqrt{3c/2} e^{-|x-ct|}$ with $c > 0$ of the mCH equation (9), which is a *right-going* travelling wave solution, and bright peakon solution. We here consider the stationary peakon solution at $t = 0$ as the initial condition

$$u(x, 0) = \sqrt{3c/2} e^{-|x|}, \quad x \in [-L, L], \quad (29)$$

and the periodic boundary $u(-L, t) = u(L, t)$. The considered PINN $f_{mch}(x, t)$ is written as

$$f_{mch}(x, t) := u_t - u_{xxt} + [(u^2 - u_x^2)(u - u_{xx})]_x. \quad (30)$$

We here consider $c = 0.04$ in the initial condition (29), and use the Fourier pseudo-spectral method (i.e., one can take Fourier transform in space, and choose the explicit fourth-order Runge-Kutta method in time) to simulate the mCH equation (9) with the initial value condition (29) and periodic boundary condition. The spatial region is $x \in [-10, 10]$ with 256 Fourier modes, and the temporal region is $t \in [0, 2]$ with time-step $\Delta t = 0.005$. As a

result, we produce the data-set for the PINN pertaining to the mCH equation. The training data-set used in the PINN $f_{mch}(x, t)$ consists of randomly chosen $N_{int} = 40$ points from the initial data $u(x, 0)$, $N_{end} = 20$ points from the end data $u(x, 2)$, $N_b = 20$ points pertaining to the periodic boundary data, and $N_f = 2000$ points from the spatio-temporal solution zone. Figures 5(a1) and (c1) exhibit the 2D and 3D profiles of the latent solution $\hat{u}(x, t)$ learned by a 7-hidden-layer deep PINN $f_{mch}(x, t)$ with 20 neurons per layer combined with a hyperbolic tangent activation function. The comparison of learning solution (red dashed line), numerical solution (blue solid line) and exact solution (green plus) is shown at three different times $t = 0.2, 1$, and 1.8 (see Fig. 5(b1)). The \mathbb{L}_2 -norm error between learning solution $\hat{u}(x, t)$ and numerical solution is $4.74\text{e-}02$.

Case 2. The mCH equation has the periodic peakon solution [40] $u(x, t) = \sqrt{3c/(2 \cosh^2 \pi + 1)} \cosh(x - ct - 2\pi[(x - ct)/(2\pi)] - \pi)$ with $c > 0$. We consider the stationary periodic peakon solution at $t = 0$ as the initial value condition

$$u(x, 0) = \sqrt{\frac{3c}{2 \cosh^2 \pi + 1}} \cosh\left(x - 2\pi \left\lfloor \frac{x}{2\pi} \right\rfloor - \pi\right), \quad c > 0 \quad (31)$$

and the periodic boundary $u(L_1, t) = u(L_2, t)$, as well as $c = 0.06$. Similarly, we use the pseudo-spectral approach to generate the data-set for the PINN pertaining to the mCH equation (9) in the spatio-temporal region $(x, t) \in [-3\pi, 3\pi] \times [0, 1]$ with the 512 Fourier modes in the x direction and time-step $\Delta t = 0.002$. The training data-set used in the PINN consists of randomly chosen $N_{int} = 60$ points from the initial data $u(x, 0)$, $N_{end} = 0$ point from the end data $u(x, 1)$, $N_b = 10$ points pertaining to the periodic boundary data, and $N_f = 2000$ points from the spatio-temporal solution zone. The hidden solution $\hat{u}(x, t)$ is learned by a 6-hidden-layer deep PINN $f_{mch}(x, t)$ with 20 neurons per layer combined with a hyperbolic tangent activation function.

Figures 5(a2) and (c2) exhibit the 2D and 3D profiles of the latent solution $\hat{u}(x, t)$ learned by a 6-hidden-layer deep PINN $f_{mch}(x, t)$ with 20 neurons per layer combined with a hyperbolic tangent activation function. The comparison of learning solution (red dashed line), numerical solution (blue solid line) and exact solution (green plus) is shown at three different times $t = 0.1, 0.5$ and 0.9 (see Fig. 5(b2)). The \mathbb{L}_2 -norm error between learning solution $\hat{u}(x, t)$ and numerical solution is $4.09\text{e-}02$.

3.5 The mCH-CH equation with both quadratic and cubic nonlinearities

Case 1. The mCH-CH equation (11) has the peakon solution [9] $u(x, t) = (-3k_2 \pm \sqrt{9k_2^2 + 24ck_1})/(4k_1)e^{-|x-ct|}$, which is a *right-going* ($c > 0$ and $9k_2^2 + 24ck_1 > 0$) or *left-going* ($c < 0$ and $9k_2^2 + 24ck_1 > 0$) peaked travelling wave solution. We here consider the stationary peakon solution at $t = 0$ as the initial condition

$$u(x, 0) = \frac{-3k_2 + \sqrt{9k_2^2 + 24ck_1}}{4k_1} e^{-|x|}, \quad (32)$$

and the periodic boundary $u(-L, t) = u(L, t)$. The considered PINN $f_{mch2}(x, t)$ is written as

$$f_{mch2}(x, t) := u_t - u_{xxt} + k_1[(u^2 - u_x^2)(u - u_{xx})]_x + k_2(3uu_x - 2u_xu_{xx} - uu_{xxx}). \quad (33)$$

i) For $c = 0.5$, $k_1 = -0.2$ and $k_2 = 2$ in the initial condition (32), which is a bright peakon solution, we use the Fourier pseudo-spectral method (i.e., one can take Fourier transform in space, and choose the explicit fourth-order Runge-Kutta method in time) to simulate the mCH-CH equation (11) with the initial value condition (32) and periodic boundary condition. The spatial region is $x \in [-10, 10]$ with 640 Fourier modes, and the temporal region is $t \in [0, 2]$ with time-step $\Delta t = 0.004$. As a result, we produce the data-set for the PINN pertaining to the mCH-CH equation. The training data-set used in the PINN $f_{mch2}(x, t)$ consists of randomly chosen $N_{int} = 40$ points from the initial data $u(x, 0)$, $N_{end} = 10$ points from the end data $u(x, 2)$, $N_b = 10$ points pertaining to the periodic boundary data, and $N_f = 5000$ points from the spatio-temporal solution zone. Figures 6(a1) and (c1) exhibit the 2D and 3D profiles of the latent solution $\hat{u}(x, t)$ learned by a 5-hidden-layer deep PINN $f_{mch2}(x, t)$ with 10 neurons per layer combined with a hyperbolic tangent activation function. The comparison of learning

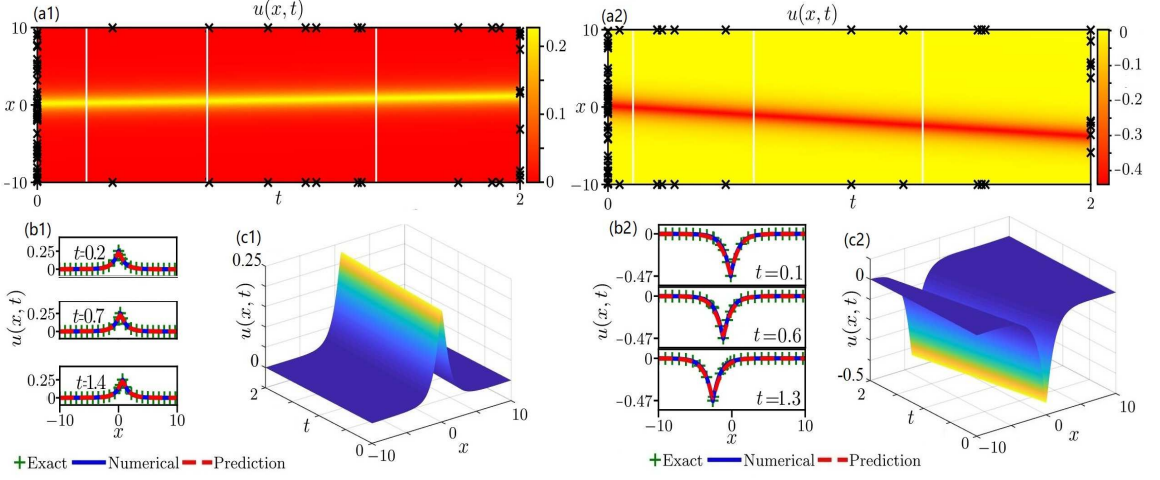


Figure 6: The mCH-CH equation with peakon solutions: (a1,a2) The data-driven peakon solution resulted from the PINN; (b1,b2) The comparisons between the learning, numerical, and exact peakon solutions at the distinct times (b1) $t = 0.2, 0.7,$ and 1.4 , (b2) $t = 0.1, 0.6,$ and 1.3 . The \mathbb{L}_2 -norm errors $\hat{u}(x, t)$ between learning and numerical peakon solutions are (b1) $6.02\text{e-}02$ and (b2) $8.47\text{e-}02$; (c1,c2) The 3D profiles of the learning bright and dark peakon solutions. $c = 0.5, k_1 = -0.2, k_2 = 2$ for (a1, b1, c1) and $c = -2, k_1 = -0.6, k_2 = 4$ for (a2, b2, c2).

solution (red dashed line), numerical solution (with blue solid line) and exact solution (green plus) is shown at three different times $t = 0.2, 0.7,$ and 1.4 (see Fig. 6(b1)). The \mathbb{L}_2 -norm error between learning solution $\hat{u}(x, t)$ and numerical solution is $6.02\text{e-}02$.

ii) For $c = -2, k_1 = -0.6$ and $k_2 = 4$ in the initial condition (32), which is a dark peakon solution, we similarly choose the spatial region $x \in [-10, 10]$ with 640 Fourier modes, and the temporal region is $t \in [0, 2]$ with time-step $\Delta t = 0.004$. As a result, we produce the data-set for the PINN pertaining to the mCH-CH equation. The training data-set used in the PINN $f_{mch2}(x, t)$ consists of randomly chosen $N_{int} = 40$ points from the initial data $u(x, 0), N_{end} = 10$ points from the end data $u(x, 2), N_b = 10$ points pertaining to the periodic boundary data, and $N_f = 6000$ points from the spatio-temporal solution zone. Figures 6(a2) and (c2) exhibit the 2D and 3D profiles of the latent solution $\hat{u}(x, t)$ learned by a 6-hidden-layer deep PINN $f_{mch2}(x, t)$ with 10 neurons per layer combined with a hyperbolic tangent activation function. The comparison of learning solution (red dashed line), numerical solution (blue solid line) and exact solution (green plus) is shown at three different times $t = 0.1, 0.6,$ and 1.3 (see Fig. 6(b2)). The \mathbb{L}_2 -norm error between learning solution $\hat{u}(x, t)$ and numerical solution is $8.47\text{e-}02$.

Case 2. The mCH-CH equation has the periodic peakon solution $u(x, t) = (-3k_2 \cosh \pi \pm a) / [2k_1(2 \cosh^2 \pi + 1)] \cosh(x - ct - 2\pi[(x - ct)/(2\pi)] - \pi)$ with $a = \sqrt{9k_2^2 \cosh^2 \pi + 12ck_1(2 \cosh^2 \pi + 1)}$. We here consider the stationary periodic peakon solution at $t = 0$ as the initial condition

$$u(x, 0) = \frac{-3k_2 \cosh \pi + \mu \sqrt{9k_2^2 \cosh^2 \pi + 12ck_1(2 \cosh^2 \pi + 1)}}{2k_1(2 \cosh^2 \pi + 1)} \cosh\left(x - 2\pi \left\lfloor \frac{x}{2\pi} \right\rfloor - \pi\right), \quad \mu = \pm 1 \quad (34)$$

and the periodic boundary condition $u(L_1, t) = u(L_2, t)$

i) We consider $\mu = 1, c = 1.5, k_1 = -0.5,$ and $k_2 = 2$ in the initial condition (34), and use the pseudo-spectral approach to generate the data-set for the PINN pertaining to the mCH-CH equation in the spatio-temporal region $(x, t) \in [-75\pi/32, 117\pi/32] \times [0, 2]$ with the 640 Fourier modes in the x direction and time-step $\Delta t = 0.004$. The training data-set used in the PINN consists of randomly chosen $N_{int} = 90$ points from the initial data $u(x, 0), N_{end} = 0$ point from the end data $u(x, 2), N_b = 10$ points pertaining to the periodic boundary data, and $N_f = 6000$ points from the spatio-temporal solution zone. The hidden solution $\hat{u}(x, t)$ is learned by a 6-hidden-layer deep PINN $f_{mch2}(x, t)$ with 40 neurons per layer combined with a hyperbolic tangent activation function.

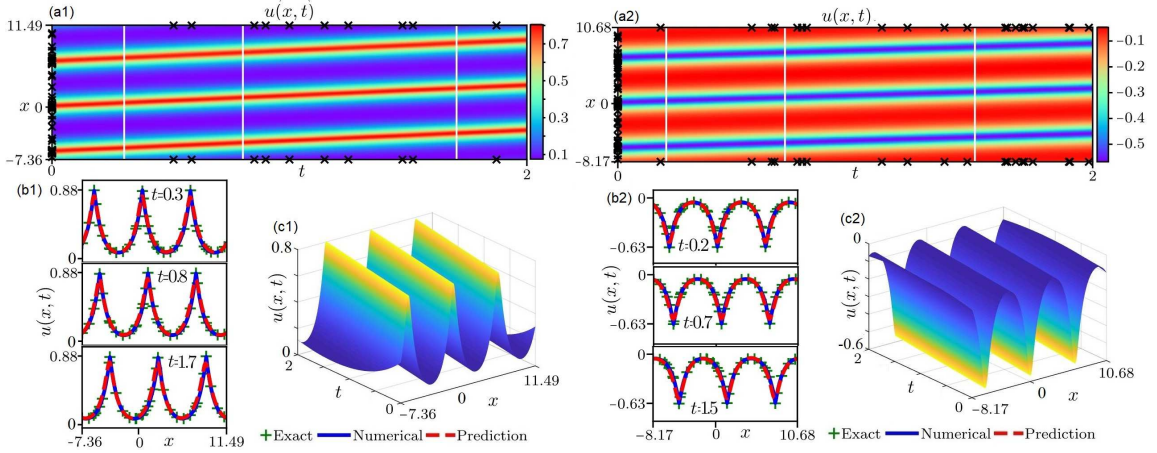


Figure 7: The mCH-CH equation. (a1,a2) The data-driven periodic peakon solution resulted from the PINN; (b1,b2) The comparisons between the learning, numerical, and exact periodic peakon solutions at the distinct times (b1) $t = 0.3, 0.8$, and 1.7 , (b2) $t = 0.2, 0.7$, and 1.5 . The \mathbb{L}_2 -norm errors $\hat{u}(x, t)$ between learning and numerical peakon solutions are (b1) $7.35\text{e-}02$ and (b2) $7.99\text{e-}02$; (c1,c2) The 3D profiles of the learning bright and dark peakon solutions. $\mu = 1, c = 1.5, k_1 = -0.5, k_2 = 2$ for (a1, b1, c1) and $\mu = -1, c = 1, k_1 = -1, k_2 = -2$ for (a2, b2, c2).

Figures 7(a1) and (c1) exhibit the 2D and 3D profiles of the latent solution $\hat{u}(x, t)$ learned by a 6-hidden-layer deep PINN $f_{mch2}(x, t)$ with 40 neurons per layer combined with a hyperbolic tangent activation function. The comparison of learning solution (red dashed line), numerical solution (blue solid line) and exact solution (green plus) is shown at three different times $t = 0.3, 0.8$ and 1.7 (see Fig. 7(b1)). The \mathbb{L}_2 -norm error between learning solution $\hat{u}(x, t)$ and numerical solution is $7.35\text{e-}02$.

ii) Similarly, we consider $\mu = -1, c = 1, k_1 = -1$, and $k_2 = -2$ in the initial condition (34), use the pseudo-spectral approach to generate the data-set for the PINN pertaining to the mCH-CH equation in the spatio-temporal region $(x, t) \in [-2.6\pi, 3.4\pi] \times [0, 2]$ with the 640 Fourier modes in the x direction and time-step $\Delta t = 0.004$. The training data-set used in the PINN consists of randomly chosen $N_{int} = 90$ points from the initial data $u(x, 0)$, $N_{end} = 0$ points from the end data $u(x, 2)$, $N_b = 20$ points pertaining to the periodic boundary data, and $N_f = 6000$ points from the spatio-temporal solution zone. The hidden solution $\hat{u}(x, t)$ is learned by a 6-hidden-layer deep PINN $f_{mch2}(x, t)$ with 40 neurons per layer combined with a hyperbolic tangent activation function.

Figures 7(a2) and (c2) exhibit the 2D and 3D profiles of the latent solution $\hat{u}(x, t)$ learned by a 6-hidden-layer deep PINN $f_{mch2}(x, t)$ with 40 neurons per layer combined with a hyperbolic tangent activation function. The comparison of learning solution (red dashed line), numerical solution (blue solid line) and exact solution (green plus) is shown at three different times $t = 0.2, 0.7$ and 1.5 (see Fig. 7(b2)). The \mathbb{L}_2 -norm error between learning solution $\hat{u}(x, t)$ and numerical solution is $7.99\text{e-}02$.

3.6 The mCH-Novikov equation with cubic nonlinearity

In the subsection, we use the PINN to consider the data-driven peakon and periodic peakon solutions of the initial-boundary value problem of the mCH-Novikov equation (12).

Case 1. The mCH-Novikov equation (12) has the peakon solution [11] $u(x, t) = \sqrt{3c/(2k_1 + 3k_2)}e^{-|x-ct|}$, which is a *right-going* for $c > 0, 2k_1 + 3k_2 > 0$ or *left-going* for $c < 0, 2k_1 + 3k_2 < 0$ peaked travelling wave solution. We here consider the stationary peakon solution at $t = 0$ as the initial condition

$$u(x, 0) = \sqrt{3c/(2k_1 + 3k_2)}e^{-|x|}, \quad c > 0, \quad (35)$$

and the periodic boundary $u(-L, t) = u(L, t)$. The considered PINN $f_{mchn}(x, t)$ is written as

$$f_{mchn}(x, t) := u_t - u_{xxt} + k_1[(u^2 - u_x^2)(u - u_{xx})]_x + k_2(4u^2u_x - 3uu_xu_{xx} - u^2u_{xxx}). \quad (36)$$

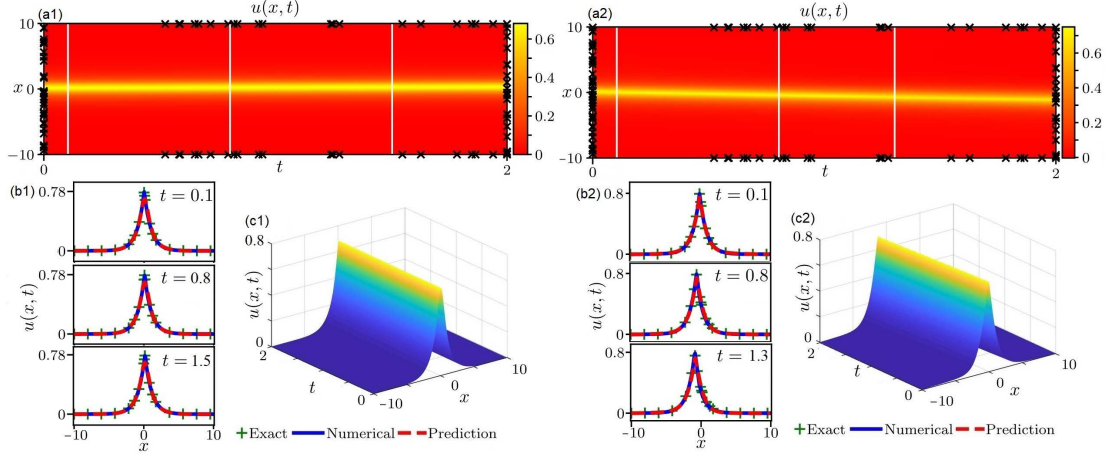


Figure 8: The mCH-Novikov equation. (a1,a2) The data-driven peakon solution resulted from the PINN; (b1,b2) The comparisons between the learning, numerical, and exact peakon solutions at the distinct times (b1) $t = 0.1, 0.8,$ and $1.5,$ (b2) $t = 0.1, 0.8,$ and $1.3.$ The \mathbb{L}_2 -norm errors $\hat{u}(x, t)$ between learning and numerical peakon solutions are (b1) $6.02\text{e-}02$ and (b2) $1.31\text{e-}02;$ (c1,c2) The 3D profiles of the learning bright peakon solutions. $c = 0.1, k_1 = -0.25, k_2 = 1/3$ for (a1, b1, c1) and $c = -0.7, k_1 = -0.15, k_2 = -1$ for (a2, b2, c2).

i) For $c = 0.1, k_1 = -0.25$ and $k_2 = 1/3$ in the initial condition (35), which is a bright peakon solution, we use the Fourier pseudo-spectral method (i.e., one can take Fourier transform in space, and choose the explicit fourth-order Runge-Kutta method in time) to simulate the mCH-Novikov equation (12) with the initial value condition (35) and periodic boundary condition. The spatial region is $x \in [-10, 10]$ with 256 Fourier modes, and the temporal region is $t \in [0, 2]$ with time-step $\Delta t = 0.004.$ As a result, we produce the data-set for the PINN pertaining to the mCH-Novikov equation. The training data-set used in the PINN $f_{mchn}(x, t)$ consists of randomly chosen $N_{int} = 30$ points from the initial data $u(x, 0), N_{end} = 20$ points from the end data $u(x, 2), N_b = 20$ points pertaining to the periodic boundary data, and $N_f = 1000$ points from the spatio-temporal solution zone. Figures 8(a1) and (c1) exhibit the 2D and 3D profiles of the latent solution $\hat{u}(x, t)$ learned by a 7-hidden-layer deep PINN $f_{mchn}(x, t)$ with 10 neurons per layer combined with a hyperbolic tangent activation function. The comparison of learning solution (red dashed line), numerical solution (blue solid line) and exact solution (green plus) is shown at three different times $t = 0.1, 0.8,$ and 1.5 (see Fig. 8(b1)). The \mathbb{L}_2 -norm error between learning solution $\hat{u}(x, t)$ and numerical solution is $6.02\text{e-}02.$

ii) We here consider $c = -0.7, k_1 = -0.15$ and $k_2 = -1$ in the initial condition (35) such that the initial condition is a bright peakon. Similarly, we choose the spatial region $x \in [-10, 10]$ with 256 Fourier modes, and the temporal region is $t \in [0, 2]$ with time-step $\Delta t = 0.004.$ As a result, we produce the data-set for the PINN pertaining to the mCH-Novikov equation. The training data-set used in the PINN $f_{mchn}(x, t)$ consists of randomly chosen $N_{int} = 50$ points from the initial data $u(x, 0), N_{end} = 20$ points from the end data $u(x, 2), N_b = 20$ points pertaining to the periodic boundary data, and $N_f = 1000$ points from the spatio-temporal solution zone. Figures 8(a2) and (c2) exhibit the 2D and 3D profiles of the latent solution $\hat{u}(x, t)$ learned by a 6-hidden-layer deep PINN $f_{mchn}(x, t)$ with 10 neurons per layer combined with a hyperbolic tangent activation function. The comparison of learning solution (red dashed line), numerical solution (with blue solid line) and exact solution (green plus) is shown at three different times $t = 0.1, 0.8,$ and 1.3 (see Fig. 8(b2)). The \mathbb{L}_2 -norm error between learning solution $\hat{u}(x, t)$ and numerical solution is $1.31\text{e-}02.$

Case 2. The mCH-Novikov equation (12) can be shown to possess the periodic peakon solution $u(x, t) = \sqrt{3c/[k_1(2 \cosh^2 \pi + 1) + 3k_2 \cosh^2 \pi]} \cosh(x - ct - 2\pi[(x - ct)/(2\pi)]) - \pi$ with $c > 0.$ We consider the station-

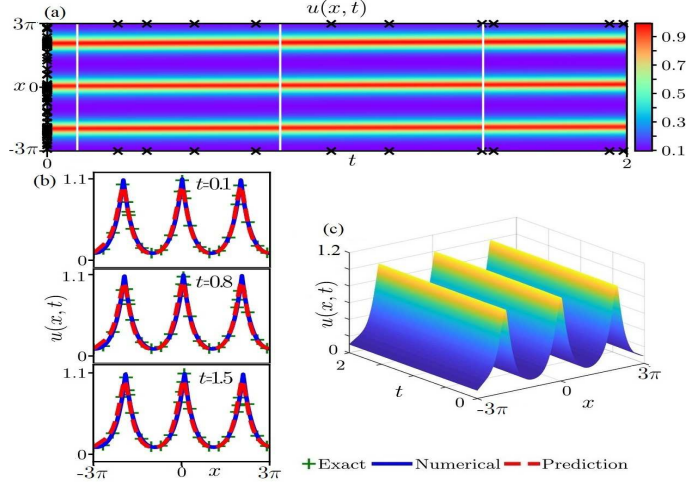


Figure 9: The mCH-Novikov equation. (a) The data-driven periodic peakon solution resulted from the PINN; (b) The comparisons between the learning, numerical, and exact periodic peakon solutions at the distinct times $t = 0.1, 0.8,$ and 1.5 . The \mathbb{L}_2 -norm error between the learning and numerical periodic peakon solutions is $8.23\text{e-}02$; (c) The 3D profile of the learning periodic peakon solution.

ary periodic peakon solution at $t = 0$ as the initial value condition

$$u(x, 0) = \sqrt{\frac{3c}{k_1(2 \cosh^2 \pi + 1) + 3k_2 \cosh^2 \pi}} \cosh\left(x - 2\pi \left\lfloor \frac{x}{2\pi} \right\rfloor - \pi\right), \quad c > 0 \quad (37)$$

and the periodic boundary condition $u(L_1, t) = u(L_2, t)$, as well as $c = 0.2, k_1 = -0.25, k_2 = 1/3$.

Similarly, we use the pseudo-spectral approach to generate the data-set for the PINN pertaining to the mCH-Novikov equation in the spatio-temporal region $(x, t) \in [-3\pi, 3\pi] \times [0, 2]$ with the 512 Fourier modes in the x direction and time-step $\Delta t = 0.004$. The training data-set used in the PINN consists of randomly chosen $N_{int} = 60$ points from the initial data $u(x, 0)$, $N_{end} = 0$ point from the end data $u(x, 2)$, $N_b = 10$ points pertaining to the periodic boundary data, and $N_f = 2000$ points from the spatio-temporal solution zone. The hidden solution $\hat{u}(x, t)$ is learned by a 6-hidden-layer deep PINN $f_{mchn}(x, t)$ with 20 neurons per layer combined with a hyperbolic tangent activation function.

Figures 9(a) and (c) exhibit the 2D and 3D profiles of the latent solution $\hat{u}(x, t)$ learned by a 6-hidden-layer deep PINN $f_{mchn}(x, t)$ with 20 neurons per layer combined with a hyperbolic tangent activation function. The comparison of learning solution (red dashed line), numerical solution (blue solid line) and exact solution (green plus) is shown at three different times $t = 0.1, 0.8$ and 1.5 (see Fig. 9(b)). The \mathbb{L}_2 -norm error between learning solution $\hat{u}(x, t)$ and numerical solution is $8.23\text{e-}02$.

3.7 The generalized mCH equation with quintic nonlinearity

In the subsection, we use the PINN to consider the data-driven peakon and periodic peakon solutions of the initial-boundary value problem of the generalized mCH equation (8) with $k = 2$.

Case 1. The generalized mCH equation (8) with $k = 2$ admits the peakon solution [41] $u(x, t) = \sqrt[4]{15c/8} e^{-|x-ct|}$ with $c > 0$. We here consider the stationary peakon solution at $t = 0$ as the initial condition

$$u(x, 0) = \sqrt[4]{\frac{15c}{8}} e^{-|x|}, \quad c > 0, \quad (38)$$

and the periodic boundary $u(-L, t) = u(L, t)$. The considered PINN $f_{gmch}(x, t)$ is written as

$$f_{gmch}(x, t) := u_t - u_{xxt} + [(u^2 - u_x^2)^2 (u - u_{xx})]_x. \quad (39)$$

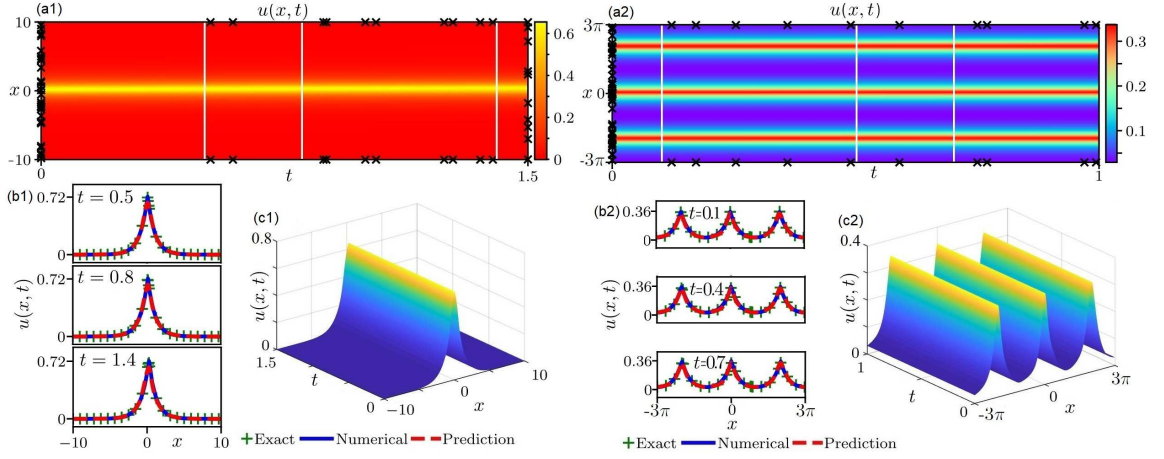


Figure 10: The generalized mCH equation (8) with $k = 2$: (a1,a2) The data-driven peakon solution resulted from the PINN; (b1, b2) The comparisons between the learning, numerical, and exact peakon solutions at the distinct times (b1) $t = 0.5, 0.8, 1.4$ or (b2) $t = 0.1, 0.4, 0.7$. The \mathbb{L}_2 -norm errors $\hat{u}(x, t)$ between learning and numerical peakon solutions are (b1) $5.29\text{e-}02$ and (b2) $3.84\text{e-}02$; (c1,c2) The 3D profiles of the learning bright peakon and periodic peakon solutions. $c = 0.15$ for (a1, b1, c1) and $c = 0.1$ for (a2, b2, c2).

We here consider $c = 0.15$ in the initial condition (40), and use the Fourier pseudo-spectral method (i.e., one can take Fourier transform in space, and choose the explicit fourth-order Runge-Kutta method in time) to simulate the generalized mCH equation (8) with $k = 2$ and the initial value condition (40) and periodic boundary condition. The spatial region is $x \in [-10, 10]$ with 640 Fourier modes, and the temporal region is $t \in [0, 1.5]$ with time-step $\Delta t = 0.003$. As a result, we produce the data-set for the PINN pertaining to the generalized mCH equation. The training data-set used in the PINN $f_{gmch}(x, t)$ consists of randomly chosen $N_{int} = 30$ points from the initial data $u(x, 0)$, $N_{end} = 10$ points from the end data $u(x, 1.5)$, $N_b = 10$ points pertaining to the periodic boundary data, and $N_f = 2000$ points from the spatio-temporal solution zone. Figures 10(a1) and (c1) exhibit the 2D and 3D profiles of the latent solution $\hat{u}(x, t)$ learned by a 5-hidden-layer deep PINN $f_{gmch}(x, t)$ with 10 neurons per layer combined with a hyperbolic tangent activation function. The comparison of learning solution (red dashed line), numerical solution (blue solid line) and exact solution (green plus) is shown at three different times $t = 0.5, 0.8$, and 1.4 (see Fig. 10(b1)). The \mathbb{L}_2 -norm error between learning solution $\hat{u}(x, t)$ and numerical solution is $5.29\text{e-}02$.

Case 2. The generalized mCH equation (8) with $k = 2$ possesses the periodic peakon solution $u(x, t) = \sqrt[4]{15c \operatorname{csch}\pi / (8 \cosh^4 \pi + 4 \cosh^2 \pi + 3)} \cosh(x - ct - 2\pi[(x - ct)/(2\pi)] - \pi)$ with $c > 0$. We consider the stationary periodic peakon solution at $t = 0$ as the initial value condition

$$u(x, 0) = \sqrt[4]{\frac{15c \operatorname{csch}\pi}{8 \cosh^4 \pi + 4 \cosh^2 \pi + 3}} \cosh\left(x - 2\pi \left\lfloor \frac{x}{2\pi} \right\rfloor - \pi\right), \quad c > 0 \quad (40)$$

and the periodic boundary condition $u(-L, t) = u(L, t)$, as well as $c = 0.1$.

Similarly, we use the pseudo-spectral approach to generate the data-set for the PINN pertaining to the generalized mCH equation (8) with $k = 2$ in the spatio-temporal region $(x, t) \in [-3\pi, 3\pi] \times [0, 1]$ with the 512 Fourier modes in the x direction and time-step $\Delta t = 0.002$. The training data-set used in the PINN consists of randomly chosen $N_{int} = 60$ points from the initial data $u(x, 0)$, $N_{end} = 0$ point from the end data $u(x, 2)$, $N_b = 10$ points pertaining to the periodic boundary data, and $N_f = 2000$ points from the spatio-temporal solution zone. The hidden solution $\hat{u}(x, t)$ is learned by a 6-hidden-layer deep PINN $f_{gmch}(x, t)$ with 20 neurons per layer combined with a hyperbolic tangent activation function.

Figures 10(a2) and (c2) exhibit the 2D and 3D profiles of the latent solution $\hat{u}(x, t)$ learned by a 6-hidden-layer deep PINN $f_{gmch}(x, t)$ with 20 neurons per layer combined with a hyperbolic tangent activation function. The

comparison of learning solution (red dashed line), numerical solution (blue solid line) and exact solution (green plus) is shown at three different times $t = 0.1, 0.4$ and 0.7 (see Fig. 10(b2)). The \mathbb{L}_2 -norm error between learning solution $\hat{u}(x, t)$ and numerical solution is $3.84\text{e-}02$.

4 Conclusions and discussions

In summary, we have applied the PINN deep learning to successfully explore the data-driven peakon and periodic peakon solutions of some nonlinear dispersive equations with some initial-boundary value conditions such as the Camassa-Holm (CH) equation, Degasperis-Procesi equation, modified CH equation, b -family equation, Novikov equation, mCH-Novikov equation, and etc. Moreover, the PINN deep learning approach can also be extended to other nonlinear peakon equations given by Eqs. (13) and (14), and higher-dimensional coupled nonlinear dispersive equations with peakon solutions. These questions will be studied in another literature.

Acknowledgements

This work is partially supported by the NSFC under Grant Nos. 11731014 and 11925108.

Appendix A. The DP equation

In the appendix, we use the PINN deep learning approach to consider the data-driven peakon and periodic peakon solutions of the initial-boundary value problem of the DP equation (4). Though the CH equation and DP equation both admit the same peakon and periodic peakon solutions, but their Lax pairs are different, where the CH equation has the second-order Lax pair [2], and the DP equation admits the third-order Lax pair [5].

Case 1. Since the DP equation (4) also admit the peakon solution [5] $u(x, t) = ce^{-|x-ct|}$, thus we consider the initial value condition (20) and periodic boundary condition $u(-L, t) = u(L, t)$. The considered PINN $f_{dp}(x, t)$ is chosen as

$$f_{dp}(x, t) := u_t - u_{xxt} + 4uu_x - 3u_xu_{xx} - uu_{xxx}. \quad (41)$$

i) We take $c = 0.6$ in the initial condition (20) and use the pseudo-spectral method to generate the data-set for the PINN pertaining to the DP equation (4) in the spatio-temporal region $(x, t) \in [-5, 5] \times [0, 3]$ with the 256 Fourier modes in the x direction and time-step $\Delta t = 0.006$. The training data-set used in the deep PINN $f_{dp}(x, t)$ consists of randomly chosen $N_{int} = 10$ points from the initial data $u(x, 0)$, $N_{end} = 10$ points from the end data $u(x, 3)$, $N_b = 10$ points pertaining to the periodic boundary data, and $N_f = 1000$ points from the spatial-temporal solution zone. The hidden solution $\hat{u}(x, t)$ can be trained by the the 5-hidden-layer deep PINN $f_{dp}(x, t)$ with 10 neurons per layer and a hyperbolic tangent activation function.

Figures 11(a1) and (c1) exhibit the 2D and 3D profiles of the latent bright-peakon solution $\hat{u}(x, t)$. The comparison of learning solution (red dashed line), numerical solution (blue solid line) and exact solution (green plus) is shown at three different times $t = 0.3, 1.5,$ and 2 (see Fig. 11(b1)). The \mathbb{L}_2 -norm error between learning solution $\hat{u}(x, t)$ and numerical solution is $2.74\text{e-}02$.

ii) For the case $c = -1.05$ in the initial condition (20), we consider the spatio-temporal region $(x, t) \in [-7, 7] \times [0, 3]$ with 256 Fourier modes and time-step $\Delta t = 0.006$. The training data-set used in the 5-hidden-layer deep PINN $f_{dp}(x, t)$ with 20 neurons per layer consists of randomly chosen $N_{int} = 10$ points from the initial data $u(x, 0)$, $N_{end} = 10$ points from the end data $u(x, 3)$, $N_b = 10$ points pertaining to the periodic boundary data, and $N_f = 1000$ points from the spatial-temporal solution zone. Figures 11(a2) and (c2) exhibit the 2D and 3D profiles of the latent solution $\hat{u}(x, t)$. The comparison of learning solution (red dashed line), numerical solution (blue solid line) and exact solution (green plus) is shown at three different times $t = 0.4, 1.3$ and 2.4 (see Fig. 11(b2)). The \mathbb{L}_2 -norm error between learning solution $\hat{u}(x, t)$ and numerical solution is $3.29\text{e-}02$.

Case 2. Since the DP equation (4) admit the same periodic peakon solution as one of the CH equation, thus we consider the initial value condition (22) with $c = -0.5$ and periodic boundary conditions. Similarly, The considered

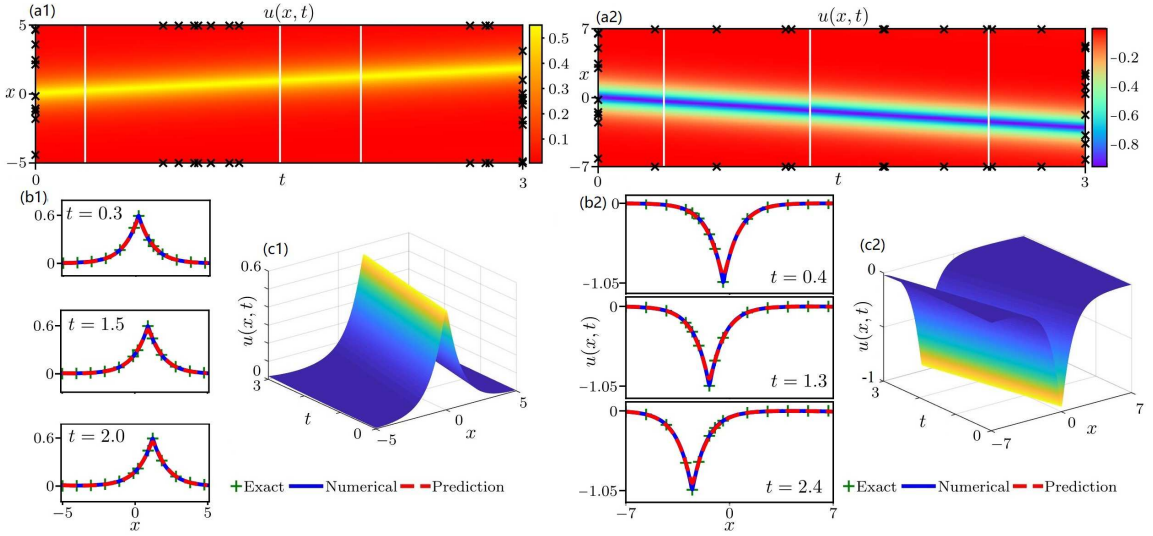


Figure 11: The DP equation. (a1,a2) The data-driven peakon solutions resulted from the PINN; (b1,b2) The comparisons between the learning, numerical, and exact peakon solutions at the distinct times (a1) $t = 0.3, 1.5,$ and $2,$ (a2) $t = 0.4, 1.3,$ and $2.4;$ The \mathbb{L}_2 -norm errors $\hat{u}(x, t)$ between learning and numerical peakon solutions are (b1) $2.74\text{e-}02$ and (b2) $3.29\text{e-}02;$ (c1,c2) The 3D profiles of the learning bright and dark peakon solutions. $c = 0.6$ for (a1, b1, c1) and $c = -1.05$ for (a2, b2, c2).

spatio-temporal region in the pseudo-spectral method is $(x, t) \in [-16\pi/5, 14\pi/5] \times [0, 2]$ with 512 Fourier modes and time-step $\Delta t = 0.004$. The training data-set used in the 6-hidden-layer deep PINN $f_{dp}(x, t)$ with 20 neurons per layer consists of randomly chosen $N_{int} = 90$ points from the initial data $u(x, 0), N_{end} = 10$ points from the end data $u(x, 2), N_b = 10$ points pertaining to the periodic boundary data, and $N_f = 1000$ points from the spatial-temporal solution zone by minimizing the MSE loss (16).

Figures 12(a) and (c) exhibit the 2D and 3D profiles of the latent periodic peakon solution $\hat{u}(x, t)$. The comparison of learning solution (red dashed line), numerical solution (with blue solid line) and exact solution (green plus) is shown at three different times $t = 0.4, 0.9,$ and 1.9 (see Fig. 12(b)). The \mathbb{L}_2 -norm error between learning solution $\hat{u}(x, t)$ and numerical solution is $1.96\text{e-}02$.

References

- [1] B. Fuchssteiner and A. S. Fokas, Symplectic structures, their Bäcklund transformation and hereditary symmetries, *Physica D* 4 (1981) 47-66.
- [2] R. Camassa and D. Holm. An integrable shallow water equation with peaked solitons, *Phys. Rev. Lett.* 71 (1993) 1661-1664.
- [3] P. J. Olver and P. Rosenau, Tri-Hamiltonian duality between solitons and solitary-wave solutions having compact support, *Phys. Rev. E* 53 (1996) 1900.
- [4] A. Degasperis and M. Procesi. Asymptotic integrability, pages 23-37. *Symmetry and perturbation theory* (Rome, 1998). World Sci. Publ., River Edge N.J., 1999.
- [5] A. Degasperis, D. D. Holm, and A. N. W. Hone, A new integrable equation with peakon solutions, *Theor. Math. Phys.* 133 (2002) 1463-1474.
- [6] D. D. Holm and M. F. Staley, Nonlinear balance and exchange of stability in dynamics of solitons, peakons, ramps/cliffs and leftons in a 1+1 nonlinear evolutionary PDE, *Phys. Lett. A* 308 (2003) 437-444.
- [7] A. S. Fokas, On a class of physically important integrable equations, *Physica D* 87 (1995) 145-150.

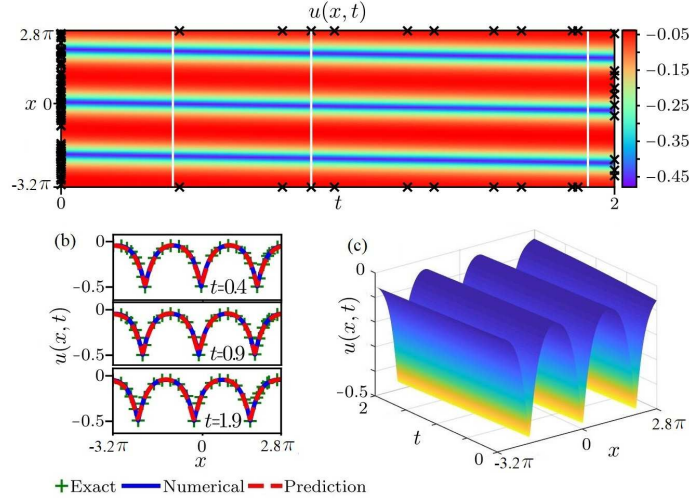


Figure 12: The DP equation. (a) The data-driven periodic peakon solution resulted from the PINN, and three distinct tested times; (b) The comparisons between the learning, numerical, and exact periodic peakon solutions at the distinct times $t = 0.4, 0.9$, and 1.9 . The \mathbb{L}_2 -norm error between the learning and numerical periodic peakon solutions is $1.96\text{e-}02$; (c) The 3D profile of the learning periodic peakon solution.

- [8] Z. Qiao, A new integrable equation with cuspons and W/M-shape-peaks solitons, *J. Math. Phys.* 47 (2006) 112701.
- [9] Z. Qiao, B. Xia, and J.B. Li, Integrable system with peakon, weak kink, and kink-peakon interactional solutions, arXiv: 1205.2028 (2012).
- [10] V. Novikov. Generalizations of the Camassa-Holm equation, *J. Phys. A* 42 (2009) 342002.
- [11] Y. Mi, Y. Liu, D. Huang, and B. Guo, Qualitative analysis for the new shallow-water model with cubic nonlinearity, *J. Differ. Equ.* 269 (2020) 5228-5279.
- [12] Y. LeCun, Y. Bengio, and G. Hinton, Deep learning, *Nature* 521 (2015) 436-444.
- [13] I. Goodfellow, Y. Bengio, A. Courville, Deep learning, MIT Press (2016).
- [14] M. Dissanayake and N. Phan-Thien. Neural-network-based approximations for solving partial differential equations, *Commun. Numer. Meth. Eng.* 10 (1994) 195-201.
- [15] I. E. Lagaris, A. Likas, and D. I. Fotiadis, Artificial neural networks for solving ordinary and partial differential equations, *IEEE transactions on Neural Networks*, 9 (1998) 987-1000.
- [16] I. E. Lagaris, A. C. Likas, and G. D. Papageorgiou. Neural-network methods for boundary value problems with irregular boundaries, *IEEE Transactions on Neural Networks*, 11 (2000) 1041-1049.
- [17] S.H. Rudy, S.L. Brunton, J.L. Proctor, and J. N. Kutz, Data-driven discovery of partial differential equations, *Sci. Adv.* 3 (2017) e1602614.
- [18] J. Sirignano and K. Spiliopoulos, DGM: A deep learning algorithm for solving partial differential equations, *J. Comput. Phys.* 375 (2018) 1339-1364.
- [19] J. Han, A. Jentzen, and W. E, Solving high-dimensional partial differential equations using deep learning, *PNAS* 115 (2018) 8505-8510.
- [20] Y. Bar-Sinai, S. Hoyer, J. Hickey, and M.P. Brenner, Learning data-driven discretizations for partial differential equations, *PNAS* 116 (2019) 15344-15349.
- [21] M. Raissi and G.E. Karniadakis, Hidden physics models: machine learning of nonlinear partial differential equations, *J. Comput. Phys.* 357 (2018) 125-141.

- [22] M. Raissi, P. Perdikaris, and G. E. Karniadakis. Physics-informed neural networks: A deep learning framework for solving forward and inverse problems involving nonlinear partial differential equations, *J. Comput. Phys.* 378 (2019) 686.
- [23] M. Raissi, A. Yazdani, and G. E. Karniadakis, Hidden fluid mechanics: Learning velocity and pressure fields from flow visualizations, *Science* 367 (2020) 1026-1030.
- [24] L. Lu, X. Meng, Z. Mao, and G. E. Karniadakis, DeepXDE: A deep learning library for solving differential equations, arXiv: 1907.04502 (2019).
- [25] Z. Mao, A. D. Jagtap, and G. E. Karniadakis, Physics-informed neural networks for high-speed flows, *Comput. Meth. Appl. Mech. Eng.* 360 (2020) 112789.
- [26] Z. Zhou and Z. Yan, Solving forward and inverse problems of the logarithmic nonlinear Schrödinger equation with PT-symmetric harmonic potential via deep learning, *Phys. Lett. A* 387 (2021) 127010.
- [27] L. Wang and Z. Yan, Data-driven rogue waves and parameter discovery in the defocusing NLS equation with a potential using the PINN deep learning, arXiv: 2012.09984 (2020).
- [28] G. Pang, L. Lu, and G. E. Karniadakis. fPINNs: Fractional physics-informed neural networks, *SIAM J. Sci. Comput.* 41 (2019) A2603-A2626.
- [29] D. Zhang, L. Guo, and G. E. Karniadakis, Learning in modal space: Solving time-dependent stochastic pdes using physics-informed neural networks, *SIAM J. Sci. Comput.* 42 (2020) A639-A665.
- [30] Y. Shin, J. Darbon, and G. E. Karniadakis, On the convergence of physics informed neural networks for linear second-order elliptic and parabolic type PDEs, arXiv:2004.01806 (2020).
- [31] S. Zhou and C. Mu, The Properties of Solutions for a Generalized b-Family Equation with Peakons, *J. Nonlinear Sci.* 23 (2013) 863-889.
- [32] K. Grayshan and A. A. Himonas, Equations with peakon traveling wave solutions, *Adv. Dyn. Syst. Appl.* 8 (2013) 217-232.
- [33] S.C. Anco, P. L. da Silva, and I.L. Freire, A family of wave-breaking equations generalizing the Camassa-Holm and Novikov equations, *J. Math. Phys.* 56 (2015) 091506.
- [34] A. Himonas and D. Mantzavinos, An ab-family of equations with peakon travelling waves, *Proc. Amer. Math. Soc.* 144 (2016) 3797-3811.
- [35] A. N W Hone and J. P. Wang, Integrable peakon equations with cubic nonlinearity, *J. Phys. A* 41 (2008) 372002.
- [36] Y. Mi and C. Mu, On the Cauchy problem for the modified Novikov equation with peakon solutions, *J. Differ. Equ.* 254 (2013) 961-982.
- [37] E. Recio and S. C. Anco, Conserved norms and related conservation laws for multi-peakon equations, *J. Phys. A* 51 (2018) 065203.
- [38] S. C. Anco and E. Recio, A general family of multi-peakon equations and their properties, *J. Phys. A* 52 (2019) 125203.
- [39] G. Gui, Y. Liu, P. J. Olver, and C. Qu, Wave-breaking and peakons for a modified Camassa-Holm equation, *Commun. Math. Phys.* 319 (2013) 731-759.
- [40] C. Qu, X. Liu, and Y. Liu, Stability of peakons for an integrable modified Camassa-Holm equation with cubic nonlinearity, *Commun. Math. Phys.* 322 (2013) 967-997.
- [41] Z. Guo, X. Liu, et al., Stability of peakons for the generalized modified Camassa-Holm equation, *J Differ. Equ.* 266 (2019) 7749-7779.
- [42] M. Abadi, A. Agarwal, P. Barham, E. Brevdo, Z. Chen, C. Citro, G. S. Corrado, A. Davis, J. Dean, M. Devin, et al., TensorFlow: Large-Scale Machine Learning on Heterogeneous Distributed Systems, *Operating Systems Design and Implementation (OSDI)*, arXiv:1603.04467v2 (2016).

- [43] A. G. Baydin, B. A. Pearlmutter, A. A. Radul, and J. M. Siskind, Automatic differentiation in machine learning: a survey, *J. Machine Learning Research* 18 (2018) 1-43.
- [44] D. C. Liu and J. Nocedal, On the limited memory BFGS method for large scale optimization, *Math. Program* 45 (1989) 503-528.
- [45] L N. Trefethen, *Spectral methods in MATLAB* (SIAM, 2000).
- [46] K. Grayshan, Peakon solutions of the Novikov equation and properties of the data-to-solution map, *J. Math. Anal. Appl.* 397 (2013) 515.